American Mineralogist, Volume 103, pages 2032–2035, 2018

LETTER

How geometry and anisotropy affect residual strain in host-inclusion systems: Coupling experimental and numerical approaches

NICOLA CAMPOMENOSI[1], MATTIA L. MAZZUCCHELLI[2], BORIANA MIHAILOVA[3], MARCO SCAMBELLURI[1], ROSS J. ANGEL[2], FABRIZIO NESTOLA[4], ALESSANDRO REALI[5], AND MATTEO ALVARO[2,*]

[1]Department of Earth Science, Environment, and Life, University of Genoa, Corso Europa 26, 16132 Genoa, Italy
[2]Department of Earth and Environmental Sciences, University of Pavia, Via A. Ferrata, 1 I-27100 Pavia, Italy
[3]Department of Earth Sciences, University of Hamburg, Grindelallee 48, D-20146 Hamburg, Germany
[4]Department of Geosciences, University of Padova, Via G. Gradenigo 6, I-35131 Padova, Italy
[5]Department of Civil Engineering and Architecture, University of Pavia, Via A. Ferrata 3, I-27100 Pavia, Italy

ABSTRACT

Raman spectroscopy provides information on the residual strain state of host-inclusion systems that, coupled with the elastic geobarometry theory, can be used to retrieve the *P-T* conditions of inclusion entrapment. In situ Raman measurements of zircon and coesite inclusions in garnet from the ultrahigh-pressure Dora Maira Massif show that rounded inclusions exhibit constant Raman shifts throughout their entire volume. In contrast, we demonstrate that Raman shifts can vary from the center to the edges and corners of faceted inclusions. Step-by-step polishing of the garnet host shows that the strain in both rounded and prismatic inclusions is gradually released as the inclusion approaches the free surface of the host. More importantly, our experimental results coupled with selected numerical simulations demonstrate that the magnitude and the rate of the strain release also depend on the contrast in elastic properties between the host and the inclusion and on the inclusion crystallographic orientation with respect to the external surface. These results allowed us to give new methodological guidelines for determining the residual strain in host inclusion systems.

Keywords: Elastic barometry, inclusion, Raman spectroscopy, zircon, garnet, coesite, Dora Maira Massif, ultrahigh-pressure metamorphism

INTRODUCTION

Elastic geobarometry for host-inclusion systems is based on measurements of the residual strains produced during exhumation as a consequence of the contrast in elastic properties between the host and the inclusion. The residual strain in the inclusions can be measured by micro-Raman spectroscopy or X-ray diffraction and can be used to provide estimates of pressure and temperature (*P-T*) conditions for metamorphic rocks that are not dependent on chemical equilibrium (e.g., Rosenfeld and Chase 1961; Enami et al. 2007; Angel et al. 2015; Anzolini et al. 2018; Murri et al. 2018). Models for elastic geobarometry only apply to the simple case of elastically isotropic host-inclusion pairs with a simple ideal geometry where a small spherical inclusion is trapped in an infinite host (Angel et al. 2015). Recent numerical models showed that any deviations from the idealized geometry significantly affects the estimation of "residual pressure" (Mazzucchelli et al. 2018). Indeed, gradients in non-spherical inclusions have been already reported (e.g., Zhukov and Korsakov 2015; Murri et al. 2018). Moreover, several studies pointed out the effects on the residual "pressure" determination of the inclusion size and its partial exposure with respect to the mineral host surface (e.g., Rosenfeld and Chase 1961; Zhang 1998; Enami et al. 2007; Mazzucchelli et al. 2018). Nevertheless, open questions still remain, including: what is the effect of the inclusion anisotropy on the residual strain release? How much can the contrast in properties between the host and the inclusion and their geometry influence the residual strain? Therefore, we propose an alternative way to test the effect of the geometry of the host-inclusion system on the Raman signal and on the calculated residual pressure upon polishing: to collect spectra from selected inclusions with different shape, size, and crystallographic orientation, while performing several steps of polishing of the rock thick-section to bring the inclusion closer to the external surface of the host.

In this manuscript we report the Raman spectra of rounded and elongated zircon inclusions and a rounded coesite inclusion in pyrope from the ultrahigh-pressure (UHP) Alpine Dora Maira Massif measured before and after several subsequent steps of polishing. The measured "residual pressures" are compared with the results of a set of Finite Element models following the approach of Mazzucchelli et al. (2018). This allows us to provide new methodological guidelines and examples of correction curves to adjust measurements carried out on faceted and anisotropic inclusions and/or close to the host surface.

SAMPLE DESCRIPTION

We analyzed zircon and coesite inclusions within pyrope megablasts and porphyroblasts, respectively, from the whiteschist of the Brossasco-Isasca UHP unit in the Gilba locality, whose petrography and petrology were reported by several authors (e.g., Chopin 1984; Hermann 2003). Whiteschists occur as lenses inside

* E-mail: matteo.alvaro@unipv.it

orthogneiss and paragneiss of the Monometamorphic Complex (Supplemental[1] Materials) and mainly consist of quartz, phengite, kyanite, and porphyroblastic-to-megablastic pyrope-rich garnet. The Dora Maira whiteschist shows a phengite, garnet, and kyanite-bearing foliation that wraps around the garnet megablasts (up to 15 cm across). The latter contain numerous inclusions (from few micrometers to 1 mm in size) mainly of kyanite, rutile, and zircon. Garnet porphyroblasts (up to 2 mm in size) within the foliated rock matrix contain rutile, zircon, and coesite inclusions. Coesite grains are frequently surrounded by quartz rims and palisade quartz structures (Chopin 1984), but we only measured the rare monocrystalline unaltered coesite inclusions. For the application of elastic geobarometry, we selected garnet-core and rim domains unaltered and free of fractures. In these domains, the coesite and zircon inclusions are surrounded by birefringent haloes (Fig. 1), indicating that the structure of the garnet host around the inclusions is anisotropically strained.

Methods

As pointed out previously (Zhang 1998; Mazzucchelli et al. 2018), only small isolated inclusions far from any free surface of the garnet thick-sections (e.g., distance >3 radii of the inclusion) do not suffer potential strain release. Therefore, for this study we prepared polished sections of 250–260 μm thickness. We performed Raman spectroscopic measurements only on inclusions at the center of the section with a mean linear size smaller than 50 μm (i.e., considerably less than the distance to the host surface).

Micro-Raman scattering measurements were conducted in backscattering geometry with a Horiba Jobin-Yvon T64000 triple-monochromator spectrometer with a spectral resolution of ~2 cm^{-1} and instrumental accuracy in peak positions of ~0.35 cm^{-1}. For each inclusion, a series of spot measurements were carried out along the equatorial plane of the inclusion as shown in Figure 2. Details of the measurements and data processing are given in the Supplemental Materials[1].

We collected Raman spectra before and after polishing of the garnet hosts by known amounts. The inclusion distance from the surface (i.e., the distance between the equatorial plane of the inclusion and the host external surface) was estimated by means of optical focus coupled with the controlled z-position motorized microscope stage. We repeated the procedure until the inclusion was half-exposed. This allowed us to observe the "real time" evolution of the strains inside the inclusions in terms of changes in the Raman frequencies. Here we show examples of single crystals of zircon:

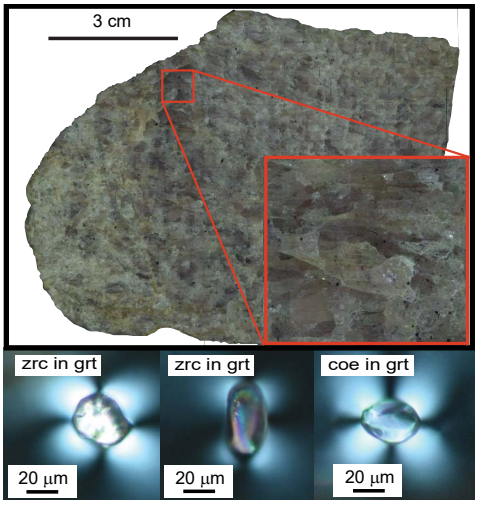

Figure 1. A polished pyrope megablast section with partial talc + chlorite alteration along fractures and rims. The red square shows an example of a millimeter-sized fracture-free garnet area selected for this study with zircon and coesite crystalline inclusions exhibiting strain-induced birefringent haloes in the surrounding host have been found.

one rounded (~20 μm radius) and one prismatic (~80 μm along the long axis), labeled S2 and S3, respectively, and one rounded, single crystal of coesite (~15 μm radius, sample S24) in the garnet megablasts and porphyroblasts, respectively. No prismatic or idiomorphic coesite inclusions have been found. Since our inclusions are elastically anisotropic, their orientation with respect to the polishing surface is critical for the interpretation of the results by means of numerical simulations. The idiomorphic zircon grain S3 has the *c* axis inclined with respect to the polishing surface by approximately 20° (estimated optically). Analysis of the peak intensities in the polarized Raman spectra suggests that the rounded zircon grain S2 has its *c* axis almost perpendicular to the surface. The coesite crystal S24 was rounded, and the absence of pronounced changes in the Raman intensities measured in different scattering geometries makes it impossible to determine its orientation, and therefore it was not possible to perform numerical simulations for this inclusion.

Finite element simulations have been carried out to support the interpretation of our measurements of zircon inclusions S2 and S3 and to evaluate the effect of the proximity of the inclusion to the external surface of the thick section on the residual strain of the inclusion (procedures as in Mazzucchelli et al. 2018, further details are reported in the data repository). Elastic anisotropy has been incorporated in the model for the zircon inclusions. The pyrope host was treated as isotropic because its universal elastic anisotropy index (Ranganathan and Ostoja-Starzewski 2008) is negligible (i.e., 9×10^{-4}), based on the elastic moduli reported by Sinogeikin and Bass (2002). The use of isotropic elastic properties for the host allows us to neglect the mutual crystallographic orientation of the host and the inclusion. For our purposes, the only relevant orientation is that of the inclusion with respect to the surface of the petrographic section.

Results and Discussion

Both rounded and idiomorphic inclusions close to the center of the section display Raman peak positions shifted toward higher wavelengths compared to free reference crystals. Within the instrumental precision (±0.35 cm^{-1}), the rounded zircon inclusion S2 and the rounded coesite inclusion S24 showed no spatial variation of the Raman peak positions within the inclusions. On the other hand, for idiomorphic crystals (zircon inclusion S3 with well-developed corners and edges) there is a steady increase in the peak positions of about 1 cm^{-1} from the center toward the edges of the inclusions (Fig. 2b). This is a direct consequence of strain heterogeneity in the inclusion, which can be caused by chemical zonation, zoned radiation-induced damage, and/or an imposed strain gradient. The substitution of elements such as Th, U, or Hf for Zr may cause expansion (U, Th) or contraction (Hf) of the zircon unit cell (Nasdala et al. 1998), leading to a change in the phonon wavenumbers. However, the compositional analysis of the exposed grain performed after the final step of polishing did not reveal any chemical zonation (see Supplemental Material[1]). Radioactive decay of elements such as U and Th can induce structural damage, leading to Raman peak broadening and a shift toward lower wavenumbers (Binvignat et al. 2018). However, the full-width at half maximum (FWHM) of a given phonon mode for totally entrapped S3 remains the same throughout the entire grain and within the instrumental spectral resolution and is equal to that of well-crystalline zircon (Binvignat et al. 2018), thus indicating a high degree of crystallinity throughout the entire grain bulk. Since the zircon inclusion S3 is chemically homogeneous (see Supplemental[1] Material) and well crystalline, the variable Raman shift in it is due to its faceted shape (Eshelby 1957), because the edges and corners act as stress concentrators (Zhang 1998; Mazzucchelli et al. 2018). After polishing the Raman spectra of S3 became homogeneous within the fully exposed part of the sample (Fig. 2b), confirming that the variation in the peak position in a single crystal for all bands was caused by the shape of the crystal.

A decrease in the Raman band wavenumbers was measured at the center of the inclusions upon polishing for all the investigated

samples of zircon and coesite. As an example, Figure 3a shows the B_{1g} mode near 1008 cm^{-1} measured on zircon sample S3 at three different steps of polishing. Strictly speaking, the phonon wavenumbers are directly related to the strain, rather than to the applied pressure. Moreover, for elastically anisotropic materials the same relative volume change can be obtained by different strains, for example as induced by hydrostatic or deviatoric stress. Therefore, the commonly used direct proportionality between the Raman peak positions and residual pressure is a strongly oversimplified assumption (Murri et al. 2018). Nonetheless, if we assume that the change in Raman wavenumber ω is linear with mean stress P (i.e., $\partial\omega/\partial P$ is constant), we can introduce the normalized change in the peak position $\Delta\omega_{norm}$ as a parameter to express the relative release in "pressure" as the inclusion becomes closer to the external surface of the host during polishing:

$$\Delta\omega_{norm} = \frac{\left(\left(\omega_{I,d}-\omega_{I,0}\right)\frac{\partial P}{\partial\omega}-\left(\omega_{I,\infty}-\omega_{I,0}\right)\frac{\partial P}{\partial\omega}\right)}{\left(\omega_{I,\infty}-\omega_{I,0}\right)\frac{\partial P}{\partial\omega}} = \frac{P_{I,d}-P_{I,\infty}}{P_{I,\infty}} = \frac{\left(\omega_{I,d}-\omega_{I,\infty}\right)}{\left(\omega_{I,\infty}-\omega_{I,0}\right)} = \Gamma \quad (1)$$

where $\omega_{I,0}$ is the wavenumber for a free crystal measured at ambient conditions, $\omega_{I,\infty}$ and $P_{I,\infty}$ are the wavenumber and the corresponding pressure for an inclusion in an infinitely large host (i.e., before the polishing, when the inclusion was far from the surface of the host), while $\omega_{I,d}$ and $P_{I,d}$ are the wavenumber measured on the inclusion and its pressure after each polishing step and associated to a specific normalized distance d (i.e., the distance from the inclusion center to the host external surface divided by the corresponding inclusion radius). Under these assumptions, Equation 1 shows that $\Delta\omega_{norm}$ becomes equivalent to the geometrical factor Γ defined by Mazzucchelli et al. (2018).

As can be seen in Figures 3b and 3c, the normalized change in the peak position $\Delta\omega_{norm}$ decreases progressively toward –1 (i.e., the Raman shift becomes equal to that of the free inclusion), when the inclusion approaches the host surface. The trends of "pressure" release estimated from the Raman spectra measured on our zircon samples show the same pattern with those calculated from numerical simulations performed on similar geometries and crystallographic orientations (e.g., see the dotted lines in Fig. 3b). However, the experimental data suggest a greater amount of stress release compared to the numerical simulations. For example, at a normalized distance of 1 (inclusion just in contact with the external surface), the calculated stress release is approximately 50%, whereas that obtained from experimental data is about 70% (Fig. 3a). There are at least two contributions to this discrepancy: (1) for non-cubic inclusions, direct conversion of Raman shifts into pressures using a hydrostatic calibration is incorrect, and (2) when the inclusion is close to the surface, strain gradients may be relaxed through plasticity or microfractures that are not considered in our purely elastic numerical models. Interestingly, our experiments show that even after partial exposure of the inclusion (i.e., for normalized distances ≤1) the Raman shift does not record full strain release (i.e., the inclusion is not at ambient conditions). In Figure 3c, for example, the polished coesite inclusion still shows 40% of its original residual strain. Finally, the difference in the strain release between zircon and coesite

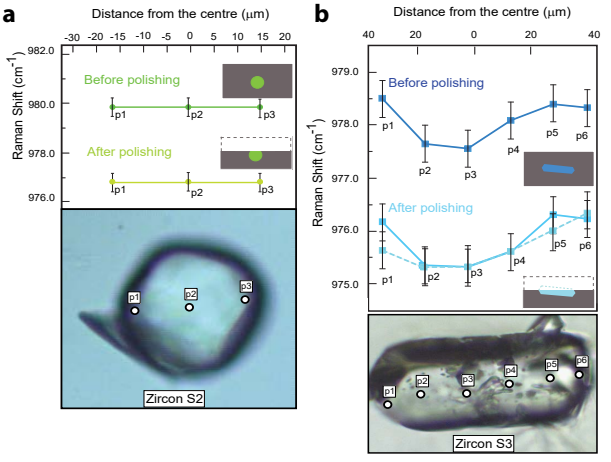

FIGURE 2. Position of the Raman peak A_{1g} at ~975 cm^{-1} in a rounded (**a**) and an idiomorphic (**b**) zircon crystal before and after the final step of polishing. The solid lines in the plots are guides for the eye; the dashed line in **b** traces the data points measured after two days of final exposure of the grain.

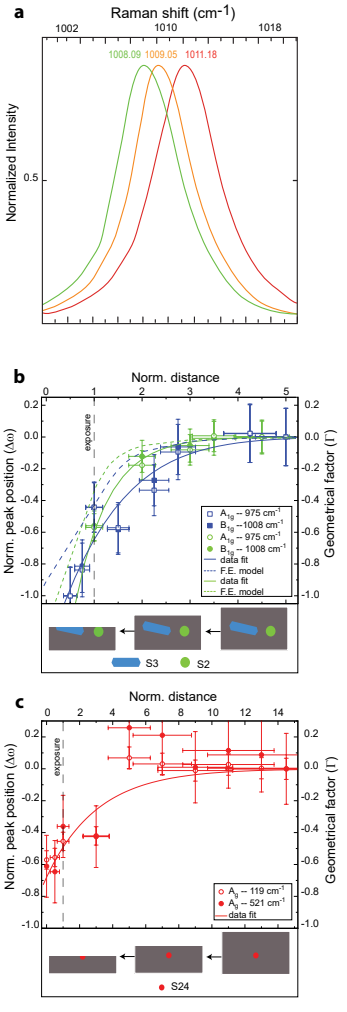

FIGURE 3. (**a**) Raman scattering arising from the antisymmetric SiO_4 stretching (the B_{1g} crystal phonon mode ~1008 cm^{-1}) measured when the grain S3 was fully entrapped (red line), at an intermediate stage of polishing (yellow), and when the inclusion was exposed at the final stage of polishing (green line). The numbers are the measured Raman shifts. (**b**) Measured normalized wavenumber shifts $\Delta\omega_{norm}$ for zircon S2 (green circles) and zircon S3 (blue squares) vs. the normalized distance d to the host surface along with Gaussian fits to the corresponding data A_{1g} of ~975 and B_{1g} ~1008 cm^{-1} data sets (solid lines) as well as the calculated geometrical factor Γ (dashed lines) from the FE model; $\Delta\omega_{norm}(d)$ and $\Gamma(d)$ show the same trend within uncertainties. (**c**) Measured $\Delta\omega_{norm}(d)$ (red circles) and a Gaussian fit to A_{1g} of ~119 and ~521 cm^{-1} (solid line) for S24 coesite inclusion.

inclusions is probably due to the different contrast in properties with respect to the host garnet. Indeed, since coesite is softer than zircon, the host garnet can still retain a greater amount of its residual strain even if half of the inclusion is exposed. This implies the possibility to have thinner hosts for softer inclusions such as coesite or quartz in garnet but, however, the possibility of fracturing during polishing is high (Enami et al. 2007).

Implications

Our measurements show that Raman shift is homogeneous only in rounded inclusions while it is non-homogeneous in faceted ones (Figs. 2a and 2b), in a full agreement with numerical calculations (Mazzucchelli et al. 2018) and theory (Eshelby 1957). Therefore, multiple Raman spectra collected on faceted inclusions should not be averaged if their differences are larger than the instrumental peak precision. Instead, to avoid the effects of grain shape on Raman peak positions, only Raman spectra measured at the center of the inclusions should be used because there we can apply the geometrical correction (see Mazzucchelli et al. 2018).

Our polishing experiments confirm that the Raman shift on the inclusion decreases as the inclusion gets closer to the external surface (Rosenfeld and Chase 1961; Zhang 1998; Mazzucchelli et al. 2018). Therefore, only inclusions whose centers are distant more than 4 radii (Fig. 3b) from the section surface and internal surfaces of the host should be used. If the Raman peak positions vary from one inclusion to another, even when the inclusions are properly selected, this indicates that some other factor is responsible, such as chemical variation in the host or inclusions, or growth of the host and thus inclusion entrapment under different conditions, such as along a prograde subduction path. More importantly, our results, coupled with our FE numerical simulations, show how anisotropy (i.e., the crystallographic orientation of the inclusion with respect to the external surface) and the contrast between the inclusion and host physical properties influence the strain release during polishing. Furthermore, even when an inclusion is exposed at the surface of the host grain, it can still exhibit a variation in the peak position with respect to a free crystal, and thus residual strains and stresses (Fig. 3c). Therefore, partially entrapped grains as a strain free standard should be avoided or chosen very carefully against which to measure the Raman shifts of unexposed inclusions.

Finally, as an example, if we calculate from our experimental Raman shift values the strain and then the mean stress in the inclusion after subsequent polishing steps, following the approach given by Murri et al. (2018), the zircon S3 has an initial residual pressure (P_{inc}) before polishing of 0.5 GPa. After 55 μm of polishing (1.5 of normalized distance in Fig. 3b), when the inclusion is still buried in its garnet host, the P_{inc} drops to 0.2 GPa. A value of 0.06 GPa is recorded when the inclusion is half exposed. For zircon S2 the initial P_{inc} was about 0.9 GPa and about 0.3 GPa when the inclusion was just touching the external surface of the host. In the Supplemental Material[1], a table showing the evolution of the P_{inc} as function of the polishing for the two zircon inclusions is reported (Table S.8). For coesite no reliable data are available to give the strain state of the inclusion from the Raman peak positions.

Acknowledgments

This project received funding from the European Research Council (ERC) under the European Union's Horizon 2020 research and innovation program grant agreements 714936 to Alvaro and ERC Starting Grant no. 307322 to Nestola. Alvaro has also been supported by the MIUR-SIR (Ministry of Education, University and Research-Scientific Independence of Young Researchers, Italy) grant MILE DEEp (Mineral Inclusion Elasticity for a New Deep Subduction Geobarometer; RBSI140351). Campomenosi acknowledges the University of Genova for funding. The authors are grateful to Peter Stutz, Hamburg, for thin-section polishing and to Alessandra Gavoglio and Paolo Campanella, Genova, for the thin-section preparation, Stefanie Heidrich, Hamburg, and Laura Negretti, Genova, for help with electron microprobe analysis. We thank Ian Swainson for the precious editorial work and the three reviewers for their fruitful suggestions and comments.

References cited

Angel, R.J., Nimis, P., Mazzucchelli, M.L., Alvaro, M., and Nestola, F. (2015) How large are departures from lithostatic pressure? Constraints from host-inclusion elasticity. Journal of Metamorphic Geology, 33, 801–813.

Anzolini, C., Prencipe, M., Alvaro, M., Romano, C., Vona, A., Lorenzon, S., Smith, E.M., Brenker, F.E., and Nestola, F. (2018) Depth of formation of super-deep diamonds: Raman barometry of $CaSiO_3$-walstromite inclusions. American Mineralogist, 103, 69–74.

Binvignat, F.A.P., Malcherek, T., Angel R.J., Paulmann, C., Schlüter J., and Mihailova, B.D. (2018) Radiation-damaged zircon under high pressures. Physics and Chemistry of Minerals, https://doi.org/10.1007/s00269-018-0978-6.

Chopin, C. (1984) Coesite and pure pyrope in high-grade blueschists of the Western Alps: a first record and some consequences. Contributions to Mineralogy and Petrology, 86, 107–118.

Enami, M., Nishiyama, T., and Mouri, T. (2007) Laser Raman microspectrometry of metamorphic quartz: A simple method for comparison of metamorphic pressures. American Mineralogist, 92, 1303–1315.

Eshelby, J.D. (1957) The determination of the elastic field of an ellipsoidal inclusion and related problems. Proceedings of the Physical Society of London, Series A, 241, 376–396.

Hermann, J. (2003) Experimental evidence for diamond-facies metamorphism in the Dora-Maira massif. Lithos, 70, 163–182.

Mazzucchelli, M.L., Burnley, P., Angel, R.J., Morganti, S., Domeneghetti, M.C., Nestola, F., and Alvaro, M. (2018) Elastic geothermobarometry: Corrections for the geometry of the host-inclusion system. Geology, 46(3), 231–234.

Murri, M., Mazzucchelli M.L., Campomenosi, N., Korsakov, A.V., Prencipe, M., Mihailova, B.D., Scambelluri, M., Angel, R.J., and Alvaro, M. (2018) Raman elastic geobarometry for anisotropic mineral inclusions. American Mineralogist, 103, 1869–1872.

Nasdala, L., Pidgeon, R.T., Wolf, D., and Irmer, G. (1998) Metamictization and U-Pb isotopic discordance in single zircons: a combined Raman microprobe and SHRIMP ion probe study. Mineralogy and Petrology, 62, 1–27.

Ranganathan, S.I., and Ostoja-Starzewski, M. (2008) Universal elastic anisotropic index. Physical Review Letter, 101, 055504-1,4

Rosenfeld, J.L., and Chase, A.B. (1961) Pressure and temperature of crystallization from elastic effects around solid inclusion minerals? American Journal of Science, 259, 519–541.

Sinogeikin, S.V., and Bass, J.D. (2002) Elasticity of pyrope and majorite-pyrope solid solutions to high temperatures. Earth and Planetary Science Letters, 203, 549–555.

Zhang, Y. (1998) Mechanical and phase equilibria in inclusion–host systems. Earth and Planetary Science Letters, 157, 209–222.

Zhukov, V.P., and Korsakov, A.V. (2015) Evolution of host-inclusion systems: a visco-elastic model. Journal of Metamorphic Geology, 33(8), 815–828.

Manuscript received June 27, 2018
Manuscript accepted July 31, 2018
Manuscript handled by Ian Swainson

Endnote:

[1]Deposit item AM-18-126700, Supplemental Materials. Deposit items are free to all readers and found on the MSA web site, via the specific issue's Table of Contents (go to http://www.minsocam.org/MSA/AmMin/TOC/2018/Dec2018_data/Dec2018_data.html).